Chemical Engineering Journal 461 (2023) 141901

Contents lists available at ScienceDirect

Chemical Engineering Journal

journal homepage: www.elsevier.com/locate/cej

Efficient boron-based electrolytes constructed by anionic and interfacial co-regulation for rechargeable magnesium batteries

Juncai Long [a], Yongkang An [a], Zhongzhuo Yang [a], Ge Zhang [a], Jianyong Zhang [a], Shuangshuang Tan [b,*], Qinyou An [a,*]

[a] State Key Laboratory of Advanced Technology for Materials Synthesis and Processing, Wuhan University of Technology, Wuhan 430070, China
[b] College of Materials Science and Engineering, Chongqing University, Chongqing 400030, China

ARTICLE INFO

Keywords:
Rechargeable magnesium batteries
Boron-based electrolytes
Mg-electrolyte interface
Anion regulation

ABSTRACT

Rechargeable magnesium batteries (RMBs) based on two-electron transfer chemistry offer great opportunities for realizing high energy density storage technology. However, the lack of magnesium-compatible electrolytes is still the biggest research and development challenge. Boron-based electrolytes, as a viable solution, have always been plagued by complex synthesis processes and high costs. In this work, an efficient boron-based electrolyte was present by a facile one-step mixed reaction of $MgCl_2$, triphenyl borate [$B(OPh)_3$], and tris(pentafluorophenyl) boron (TPFPB) in tetrahydrofuran (THF). By adjusting the composition and ratio of boron-based salts in the electrolyte, a modified anion structure with lower HOMO states was obtained. Besides, the as-prepared electrolyte also contributes to the formation of MgF_2-rich solid electrolyte interphase (SEI) layer, which significantly inhibits the electrolyte decomposition, enhance the cycling stability of Mg anodes. Eventually, the electrolyte exhibits a wide electrochemical window (>3 V vs Mg/Mg^{2+}), low polarization voltage (150 mV) and an average Coulombic efficiency above 98 %. Finally, the successful assembly of the Mg/CuS and Mg/Mo_6S_8 full batteries confirms the practicability of this electrolyte in RMBs. More importantly, the dual regulation strategy of anions and interfaces offers a novel idea for designing efficient electrolytes in RMBs.

1. Introduction

The application of lithium-ion batteries (LIBs) in various fields has greatly improved the convenience of life. Nevertheless, increasingly tight world energy supply and rising environmental requirements call for next-generation energy storage technology, but LIBs cannot meet the ever-increasing demand [1–3]. Among many alternative post-lithium-ion batteries, rechargeable magnesium batteries (RMBs) based on two-electron transfer chemistry are gaining much attention caused by high theoretical capacity (3382 mAh cm^{-3} and 2205 mAh g^{-1}), high earth-abundance, low cost, and high safe (homogeneous plating morphology) of Mg metal anode [4–8]. However, the development of RMBs is still in its infancy, the lack of suitable electrolytes remains the biggest obstacle [9–12].

In RMBs system, magnesium-compatible electrolytes as a bridge between Mg anode and cathode materials have been extensively studied in the past few decades [13–15]. Compared to monovalent Li^+, Mg^{2+} has a similar ionic radius (0.66 Å to 0.68 Å). However, twice the amount of electric charge will produce more electrostatic interactions, leading to sluggish Mg^{2+} transport in the host material [16]. Besides, highly reactive Mg metal anode is passivated in the conventional electrolytes (e.g., $Mg(ClO_4)_2$, $Mg(PF_6)_2$ or $Mg(TFSI)_2$ salts in carbonate or ether solvents), which hinders the transport of Mg^{2+}, putting forward more stringent requirements for the electrolyte design [17,18]. Lewis acid-base reaction was usually used to prepare the widely accepted APC (All Phenyl Complex) [19], MACC (inorganic Magnesium Aluminum Chloride Complex) [20–22] and hexamethyldisilazide (HMDS) [23,24] based electrolytes for RMBs. However, in the above-mentioned electrolytes, the introduction of Al^{3+} ($AlCl_3$ as Lewis acid) leads to irreversible aluminum deposition during cycling [25], further reducing the Coulombic efficiency. Besides, low oxidative stability reduces their practicality. In contrast, boron-based electrolytes, such as $Mg[B(hfip)_4]_2$ [26,27], $Mg[B(Otfe)_4]_2$ [28] and so forth [29], exhibited high oxidation stability owing to the stable boron-center anions. As early as 2012, Hirano et al. developed a boron-based electrolyte with wide electrochemical windows through the Lewis acid-base reaction between tri(3,5-

* Corresponding authors.
E-mail addresses: tss@cqu.edu.cn (S. Tan), anqinyou86@whut.edu.cn (Q. An).

https://doi.org/10.1016/j.cej.2023.141901
Received 8 January 2023; Received in revised form 31 January 2023; Accepted 12 February 2023
Available online 14 February 2023

dimethylphenyl)borane (Mes_3B) and PhMgCl in tetrahydrofuran (THF) [30]. In recent years, Cui et al. proposed a series of effective boron-based electrolytes by a similar reaction between tris(hexafluoroisopropyl) borate (THFPB) and inorganic magnesium salts (MgF_2, $MgCl_2$, MgO, $Mg(BH_4)_2$) [31–33]. However, these electrolytes were limited by the relatively high cost of THFPB. Searching for cheap boron-based Lewis acids as substitutes is now the top priority. Triphenyl borate ($B(OPh)_3$) with the stable tri-coordinated benzene group is a low-cost candidate due to its strong donor–acceptor effects. Previous studies have already reported its potential as an electrolyte salt for RMBs [34]. Unfortunately, the electrolyte made of $MgCl_2$ and $B(OPh)_3$ in dimethoxyethane (DME) demonstrated poor current density of magnesium stripping/plating and a narrow electrochemical stability window. Therefore, it is necessary to further regulate the solvent and anion structure of this electrolyte for enhancing the oxidation stability and improving the SEI components.

Herein, we proposed an anion-regulated approach to introduce different boron salts as Lewis acid, and obtain an effective boron-based electrolyte (abbreviated as MFBP electrolyte) through proper salt ratio and solvent selection. Compared with pure $B(OPh)_3$ (abbreviated as MBP electrolyte), the introduction of tris(pentafluorophenyl)boron (TPFPB) can control the anionic structure of the electrolyte, improve the oxidative stability and stripping/plating Coulombic efficiency (~98 %). Density functional theory (DFT) theoretical calculations provide guidance for optimizing anions structure through tuning the highest occupied molecular orbital (HOMO) energy level. Besides, the MgF_2-rich SEI formed during cycling contributed to inhibiting side reactions, enhancing the reversibility of Mg anode. Also, the active species of the electrolyte solutions and the effect of TPFPB were characterized by nuclear magnetic resonance (NMR), electrospray ionization mass spectrum (ESI-MS), X-ray photoelectron spectroscopy (XPS), X-ray diffraction (XRD), etc. At last, we have conducted basic research on Mg/CuS and Mg/Mo_6S_8 full batteries to further illustrate the feasibility of the prepared electrolyte.

2. Results and discussion

MFBP electrolyte was synthesized through a facile one-step Lewis acid-base reaction of $B(OPh)_3$, TPFPB, and $MgCl_2$ in various solvents. Multidentate ligand solvent such as DME shows poor solubility for B $(OPh)_3$, while monodentate ligand tetrahydrofuran (THF) can dissolve it well. Therefore, THF was eventually chosen as research solvent (Fig. S1). The main reaction equations are shown below. First, Lewis acid TPFPB with strong electron-withdrawing ability preferentially reacts with $MgCl_2$ due to the substitution of -H on the benzene ring by -F. Active cation $[MgCl]^+$ and tetra-coordinated boron-based anion $[TPFPB{\cdot}Cl]^-$ were generated (equilibrium (1)). Then, the rest of $MgCl_2$ continues to react with $B(OPh)_3$, another tetra-coordinated boron-based anion $[B(OPh)_3{\cdot}Cl]^-$ was formed (equilibrium (2)). And reaction (3) represents the equilibrium between cations and unreacted $MgCl_2$ in the electrolyte.

$$TPFPB + MgCl_2 \Rightarrow TPFPB{\cdot}Cl^- + MgCl^+ \quad (1)$$

$$B(OPh)_3 + MgCl_2 \Leftrightarrow B(OPh)_3{\cdot}Cl^- + MgCl^+ \quad (2)$$

$$MgCl^+ + MgCl_2 \Leftrightarrow Mg_2Cl_3^+ \quad (3)$$

The electrostatic potential (ESP) iso-surface plots of different boron salts are associated with the electron-absorbing ability. As list in Fig. 1a, blue area represents the accumulation of negative charges, red area represents the accumulation of positive charges [35]. For $B(OPh)_3$, the negative charge distribution is concentrated on the terminal benzene ring, when it comes to TPFPB, due to the substitution effect of -F on the benzene ring, its strong electron-withdrawing ability makes the distribution of negative charges more uniform. Therefore, TPFPB has a stronger Lewis acidity and reacts with $MgCl_2$ in advance. Besides, DFT calculations were performed to obtain the molecular orbital energy levels of the electrolyte components (Fig. 1b), the results indicated that TFPPB has a lower HOMO energy level. Generally, HOMO states represent intrinsic thermodynamic stabilization of molecular, which defines oxidative stability, the lower HOMO orbital energy level, the more difficult it is for the molecular to lose electrons, so the oxidative stability is higher [36]. The lower HOMO level obtained for TPFPB suggested higher stability of this component. The stability exhibits not only on molecular, but also anion. $[TPFPB{\cdot}Cl]^-$ anion exhibits a decreased HOMO energy level and an increased transition gap energy than $[B(OPh)_3{\cdot}Cl]^-$ anion, which suggests that the oxidative stability of the electrolyte will be correspondingly improved in the presence of $[TPFPB{\cdot}Cl]^-$.

$MgCl_2$ plays a decisive role in the balance of Lewis acid-base

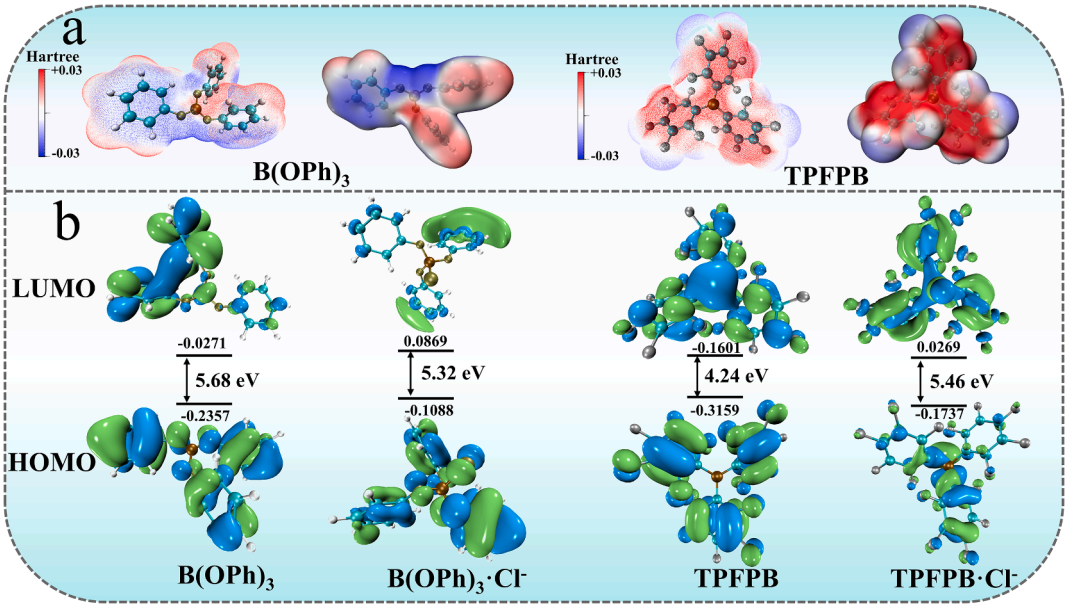

Fig. 1. Visualization of the DFT theoretical calculation. (a) ESP iso-surface of $B(OPh)_3$ and TPFPB with different degrees; the negative charge is represented in blue and the positive is represented in red. (b) Visualized LUMO/HOMO orbitals and transition gap energy of $B(OPh)_3$ and TPFPB molecules; $[B(OPh)_3{\cdot}Cl]^-$ and $[TPFPB{\cdot}Cl]^-$ anions.

reactions and the reaction products [37]. To identify the suitable ratio in this electrolyte, the Mg stripping/platting curves of several electrolytes with different concentrations of $MgCl_2$ were evaluated. When the content of $MgCl_2$ is one equivalent, this electrolyte demonstrated more pronounced peak current density and lower polarization (Fig. S2). Thus, subsequent testing and characterization were performed under this ratio. To evaluate the improved electrochemical performance of MFBP electrolyte, a series of solutions with different boron salt contents were prepared. Cyclic voltammetry curves show that the electrolyte with the addition of 20 % TPFPB has the strongest peak current density (Fig. 2a). However, when the amount of TPFPB continued to increase to 40 %, the peak current density decreased. In the case of only TPFPB as Lewis acid, the reversible stripping/platting behaviors of Mg metal could not be observed (Fig. S3). This phenomenon suggests that excess TPFPB may lead to increased surface passivation. Therefore, 20 % TPFPB was considered as the optimal ratio. Coulombic efficiency is another important parameter for assessing the practicality of electrolytes. As list in Fig. 2c, the modification of the anion structure also greatly improves the ability of the electrolyte in this aspect. The MBP electrolyte only has an average Coulombic efficiency of 85 %, and it fails quickly, while the Coulombic efficiency of the MFBP electrolyte reaches 98 % only after a few cycles of activation and stably cycled 150 times. The increased voltage hysteresis in the MBP electrolyte as shown more clearly in the capacity-voltage curves corresponding to the Coulomb efficiency, however, the voltage hysteresis of MFBP electrolyte is constantly smooth (Fig. S4).

Linear sweep voltammetry (LSV) was taken to further investigate the electrochemical oxidation stability of the MFBP electrolyte on different current collectors (Fig. 2b). The electrolyte displayed relatively low oxidation onset potentials of 1.5, 1.7, 1.9, and 2.2 V (vs Mg RE) on non-noble metal electrodes, Al, Cu, SS and Ti, respectively. These results were similar to other chlorine-containing electrolytes in previous reports due to the corrosion of chloride ions for non-noble metals [38]. However, when noble metal Mo was used as the current collector, the oxidation onset potential of MFBP reached 3.0 V. In contrast, the MBP electrolyte exhibits lower anodic stability of 2.5 V on the Mo current collector (Fig. S5). This result shows that the oxidation resistance of the electrolyte was improved by the introduction of TPFPB, which is consistent with the DFT calculation results.

Symmetric Mg//Mg cells were assembled to evaluate the polarization characteristics of Mg plating/stripping in MFBP and MBP electrolytes. With the increasing current densities, Mg stripping and plating times were maintained as 1 h per cycle. At a current density of 0.1 mA cm^{-2}, the overpotential of MFBP electrolyte was 150 mV. Then it slightly grows to 400 mV at 0.5 mA cm^{-2} (Fig. S6). Compared with MBP electrolyte, MFBP electrolyte has a smaller initial discharge potential, which means that its nucleation overpotential is lower, more conducive to the deposition of magnesium (Fig. 2d). In subsequent long-cycle tests, no large polarization differences were found between the two electrolytes for the first 80 h. However, as the cycle continues, the MBP electrolyte experienced rapidly increased overpotential (>700 mV). Moreover, the MFBP electrolyte maintained a stable overpotential of less than 150 mV even after 300 h. This significant improvement verifies that the TPFPB facilitates uniform Mg plating and stripping behaviors during the long-term cycles. It may be further affected by the anion structures and SEI components.

Electrospray ionization-mass spectrometry (ESI-MS) and ^{11}B NMR spectroscopy were employed to reveal the boron-based anion structures of electrolytes with different molar ratios. It is reported that the chemical shift in NMR spectroscopy is mainly affected by the coordination number and the electronegativity of the substituents [39]. As a list in Fig. 3a, when the $B(OPh)_3$: $MgCl_2$ was 1:1 and no TPFPB was added, ^{11}B NMR spectrum shows the two peaks at $\delta = 19.6$ ppm and $\delta = -1.2$ ppm, which are typically designated as tri-coordinated $B(OPh)_3$ and tetra-coordinated boron anion $[B(OPh)_3{\cdot}Cl]^-$. The peak with an m/z ratio of 320.7 verifies the formation of this anion (Fig. S7a). Besides, the presence of $B(OPh)_3$ in electrolyte suggests that its weaker Lewis acidity leads to an incomplete coordinating reaction with $MgCl_2$. After adding 20 % TPFPB, a strong peak at $\delta = -8.9$ ppm appeared, which was ascribed to $[TPFPB{\cdot}Cl]^-$ anion, formed by Lewis acid-base reaction

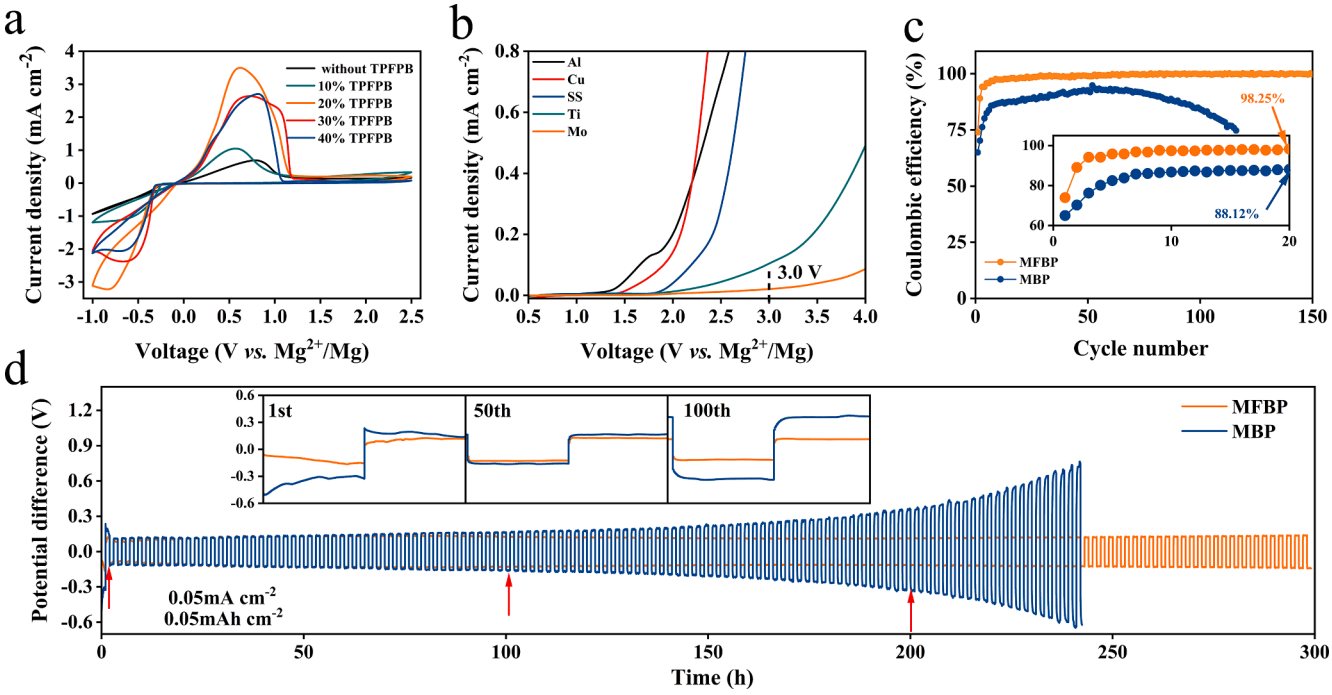

Fig. 2. (a) Cyclic voltammograms for a Mo electrode in the MFBP electrolyte with different ratios TPFPB obtained at a scanning rate of 25 mV s^{-1} in the potential range of − 1.0 V to 2.5 V vs Mg/Mg^{2+}. (b) LSVs of MFBP electrolyte on different metal electrodes. (c) Coulombic efficiency of Mg plating and stripping in MFBP and MBP electrolyte. Inset showing Coulomb efficiency for the first 20 cycles. (d) Polarization properties of Mg//Mg symmetrical cells with MBP/MFBP electrolyte at current densities of 0.05 mA cm^{-2} and 0.05 mAh cm^{-2}. The insets are the enlarged views of the first, 50th, and 100th cycles.

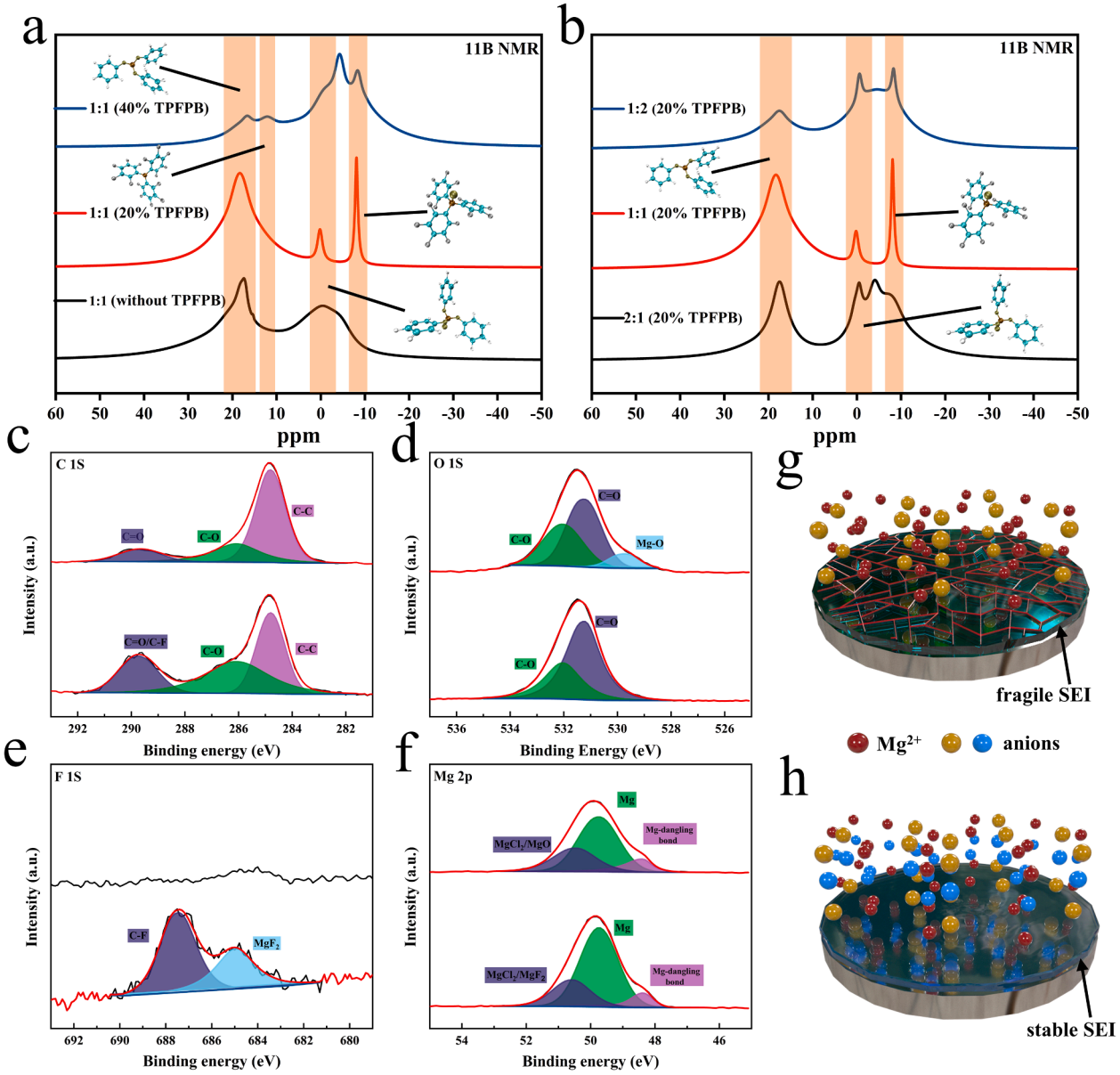

Fig. 3. ^{11}B NMR spectra of electrolyte components in THF: (a) spectrum of $B(OPh)_3$: $MgCl_2$ (1:1) and TPFPB with different molar ratios. (b) spectrum of $B(OPh)_3$: $MgCl_2$ (1:2, 1:1, 2:1) and TPFPB with 20% molar ratios. (c, d, e, f) XPS spectra of Mg foils cycled in MBP electrolytes and MFBP electrolytes for 50 times. Schematic illustration of proposed effect and morphology modulation by TPFPB modification, (g) without TPFPB, (h) with TPFPB.

between TPFPB and $MgCl_2$.The corresponding *m/z* ratio is 543.0 (Fig. S7b). The absence of extra NMR peaks indicates that TPFPB possesses a stronger Lewis acidity, so that it is fully coordinated with $MgCl_2$. Continue to increase the content of TPFPB to 40 %, a new weak peak appears at $\delta = 13.2$ ppm, which is caused by the incomplete reaction of excessive TPFPB. In addition to this, the peak of tetra-coordinated $[B(OPh)_3{\cdot}Cl]^-$ is shifted to −4.3 ppm, we speculate that this is due to the formation of $[TPFPB{\cdot}Ph]^-$ impurity. Therefore, 20 % of TPFPB is a suitable content in MFPB electrolytes. In addition, we also found no significant changes in the components of the electrolyte even after the electrochemical cycle (Fig. S8). In order to further explore the influence of Lewis acid-base ratio on electrolyte species, a series of electrolytes with different contents of $MgCl_2$ were also analyzed (Fig. 3b). When the amount of Lewis acid is in excess, the appearance of impurity peaks ($\delta = -4.3$ ppm) replaces the peaks of stable anion $[TPFPB{\cdot}Cl]^-$, which suggests that excess boron salts interfere with the reaction. Besides, when the content of $MgCl_2$ is excessed, the content of the less stable anion $[B(OPh)_3{\cdot}Cl]^-$ rises. And the peak intensity of stable anion $[TPFPB{\cdot}Cl]^-$ is not prominent, suggesting that the excessed $MgCl_2$ will also reduce the stability of the electrolyte. Above all, the addition of TPFPB contributes to the formation of $[TPFPB{\cdot}Cl]^-$ anion, which works synergistically with active ions $[B(OPh)_3{\cdot}Cl]^-$ to form an efficient and stable electrolyte.

In previous reports, TPFPB may also induce the formation of stable SEI films with lower interfacial resistance [40–42]. Therefore, XPS was performed to investigate the SEI components on Mg metal in MFPB and MPB electrolytes after 50 cycles (Fig. 3c, d, e and f). It is worth mentioning that the disassembly of the battery and the preparation and characterization of the samples were all carried out in an argon-filled glove box to prevent the interference of moisture or oxygen. The C 1 s spectrum demonstrated no significant difference, the signal of C═O (289.7 eV), C—O (286.0 eV), C—C (284.8 eV) originates from the decomposition of the electrolyte. For F 1 s spectrum, a distinct peak of MgF_2 (684.97 eV) can be detected when using MFBP electrolyte. Combined with the Mg 2p spectrum (50.4 eV), it can be inferred that there is a considerable amount of MgF_2 on the surface of the Mg anode. As an ionically conductive but electronically insulating layer, metal fluoride

can effectively prevent the decomposition of electrolyte and the occurrence of side reactions, then enhancing the cycle stability of LIBs [43,44]. Meanwhile, the MgF_2 coated layer has also been demonstrated to improve the cycling performance of Mg anode [45]. Therefore, we speculate that MgF_2 generated by the reaction of TPFPB and Mg anode plays an indispensable role in forming stable SEI layers. This is also an important reason that TPFPB can make batteries maintain long-cycle stability. Besides, as an anion receptor, TPFPB can promote the dissolution of metal oxides [46]. As the main component of Mg passivation layer, MgO always restricts the transmission of Mg^{2+}. The O 1s spectrum shows a detectable peak of MgO (529.70 eV) in the SEI of MBP electrolyte. For MFBP electrolyte, only C—O (532.0 eV) and C═O (531.3 eV) can be observed. The Mg 2p spectrum further confirmed the existence of MgO (50.4 eV) in the SEI of MBP electrolyte. This result indicates that TPFPB can also promote the dissolution of inert MgO, so that the transmission of Mg^{2+} is faster. Besides, a broad signal at 48.5 eV is assigned to Mg dangling bonds [47]. In order to further confirm the formation of SEI layer, electrochemical impedance spectroscopy (EIS) was used to characterize the resistances of the interphases in Mg//Mg cell. Before galvanostatic cycle, the cell showed high interfacial resistance, which may be caused by some inactive species adsorb and accumulate on the Mg metal surface. After electrochemical cycle, the interfacial resistance markedly decreased, besides, the new semicircle region in high frequency region corresponds to the resistance of the SEI film (R_{SEI}) (Fig. S9). More importantly, even in $Mg(TFSI)_2$-based electrolytes which severe passivation of Mg metal, the MgF_2-rich Mg metal anode can effectively suppress side reactions and the polarization of symmetric cells is significantly reduced (Fig. S10). Above all, the decomposition of electrolyte leads to proliferation of interface layer which will eventually cause high impedance of Mg^{2+} transmission, however, the formation of stable electronically insulating MgF_2-rich SEI layer and dissolution of passive components MgO allows fast ion transmission, which verifying the multifunctionality of TPFPB as an additive.

Based on the above experimental analysis, we compared the MFBP electrolyte with the reported boron-based electrolytes (Table S1) and summarized the specific mechanism of TPFPB on the surface of Mg anode, as illustrated in Fig. 3g and h. In MBP electrolyte, the stripping/plating of Mg will be accompanied by the decomposition of the electrolyte and side reactions, which leads to the formation of an unstable SEI [48]. As a result, the overpotential of ions transport gradually increases and the Coulomb efficiency of the electrolyte dropped. However, when the electrolyte component contains TPFPB, the strong Lewis acid TPFPB will react with Mg anode to form the inorganic component MgF_2. The exist of electronic insulation material MgF_2 can prevent electronic leakage and obtain a stable organic–inorganic composite MgF_2-rich SEI layer. Besides, the high ionic conductivity was not affected, allowing rapid transport of Mg ions.

Homogeneous plating morphology ensures the safety of RMBs [49]. To confirm the Mg deposition morphology in MFBP electrolyte during the electrochemical deposition process, a Mo foil was selected as a conductive substrate for Mg deposition at 0.5 mA cm^{-2} and 2 mAh cm^{-2}. XRD and scanning electron microscopy (SEM) were conducted to investigate the composition and morphology. XRD patterns (Fig. 4b) and energy dispersive spectroscopy (EDS) spectrum (Fig. 4a) confirm that sediment consists entirely of Mg polycrystals. As shown in Fig. 4c and d, the smooth and compact Mg crystals deposition morphology was determined. This result is similar to previously published results, further verifying the usability of this electrolyte.

The electrode–electrolyte compatibility is also an important factor for the feasibility of the electrolyte. CuS is a well-studied cathode material for RMBs owing to the high specific capacity and suitable voltage window [50,51]. According to our previous work, porous CuS nanoflowers synthesized by a facile one-step liquid-phase reaction [52] was chosen for full batteries characterization (Fig. S11). The Mg/CuS full batteries comprising the MBP and MFPB electrolytes were assembled and tested at room temperature. Fig. 5a presents the typical capacity-voltage profiles. In the MFBP electrolyte, the CuS cathode exhibits a

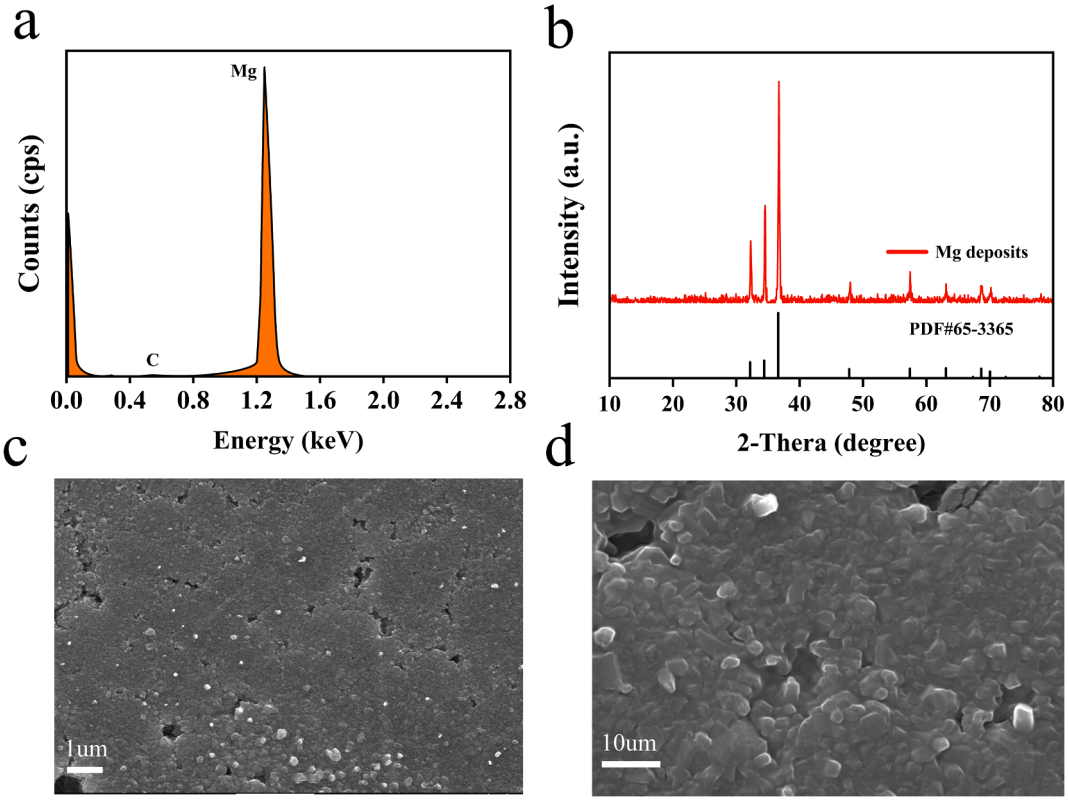

Fig. 4. (a) EDS analysis and (b) XRD result of the Mg deposits. (c and d) Typical SEM images of the Mg deposits at different magnifications.

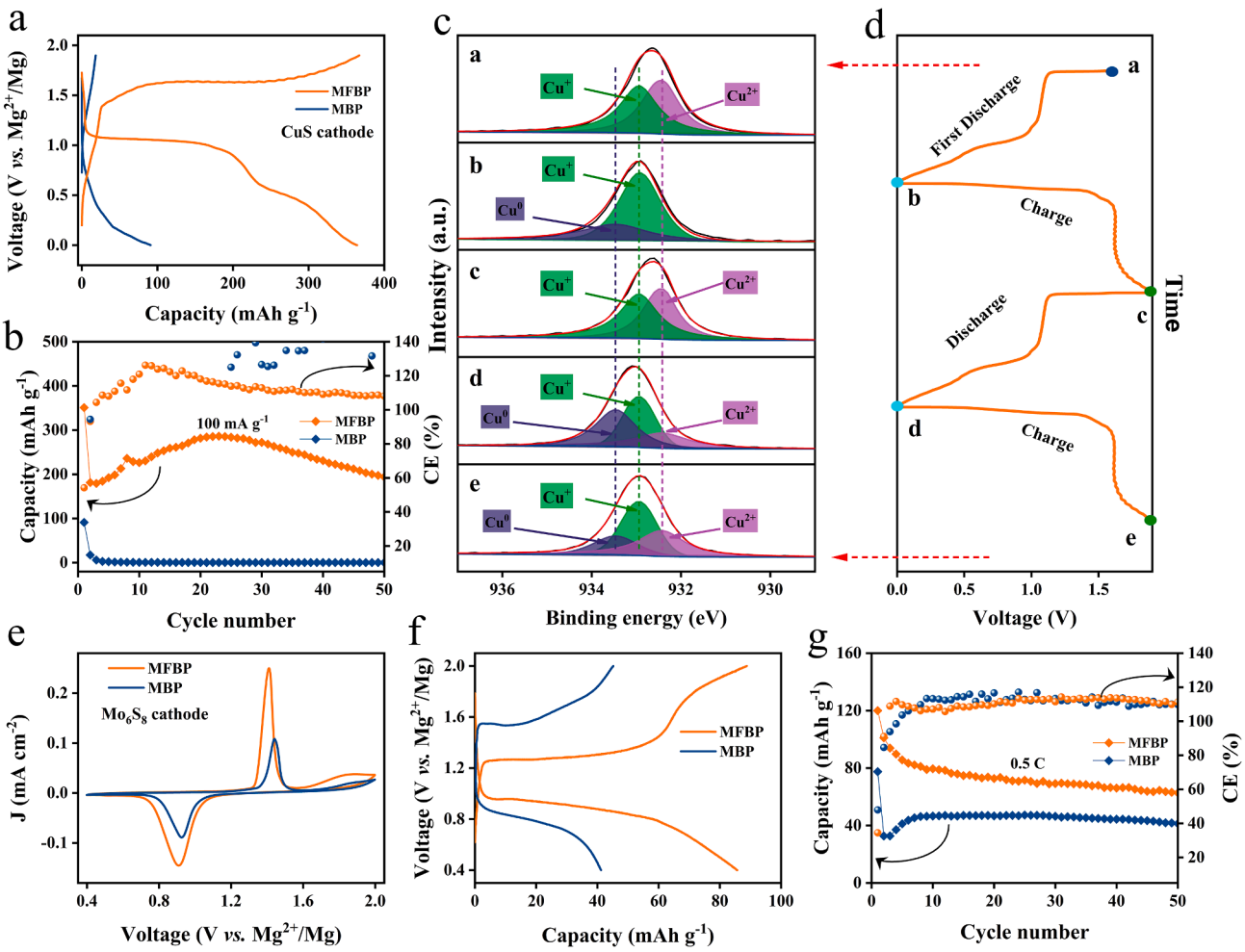

Fig. 5. (a) The representative charge/discharge curves of Mg/CuS batteries using MFPB electrolyte (orange) and MPB (blue). (b) Cycling performance and Coulombic efficiency at 100 mA g^{-1}. (c) The XPS spectra of CuS at different stages and (d) the corresponding voltage–time curves. (e) Cyclic voltammograms curves of Mg/Mo_6S_8 batteries in MFBP (orange) and MBP (blue) electrolyte at 0.1 mV s^{-1}. (f) The representative charge/discharge curves of Mg/Mo_6S_8 batteries using MFPB electrolyte (orange) and MPB (blue) at 0.5C (1C = 128.8 mAh g^{-1}). (g) Cycling performance and Coulombic efficiency at 0.5C.

more reversible two-platform magnesium storage reaction, corresponding to the conversion reaction between Mg^{2+} with CuS (1.10 V) and Cu_2S (0.55 V), respectively. However, the MBP electrolyte delivering a negligible discharge capacity in CuS cathode due to the absence of magnesium storage reaction. It is worth noting that the initial discharge capacity up to 350 mAh g^{-1} was attributed to the irreversible transformation of CuS cathode and then a highest reversible capacity of 287 mAh g^{-1} at 100 mA g^{-1} was achieved in MFBP electrolyte (Fig. 5b). In a chlorine-containing RMBs system, whether the shuttle cation is Mg^{2+} or $MgCl^+$ has always been an unavoidable issue [53]. In order to further explore the magnesium storage mechanism of the full battery, we characterized the elemental distribution in CuS cathodes at different charge–discharge states by EDS spectrum. As shown in Fig. S12, in the discharge state, due to the intercalation of Mg^{2+}, the Mg element is uniformly distributed in CuS, and in the subsequent charge state, a small part of the residual Mg element is detected. Table S2 summarizes the atomic content ratios of elements in the EDS test. Only a negligible presence of Cl element can be detected in both states, however, the content of Mg element varies with charge and discharge, so Mg^{2+} were the ions that mainly participate in the reaction. Besides, the *ex-situ* XPS spectra (Fig. 5c) was used to explore the change of Cu valence state during charging and discharging process [54]. In the initial state, both Cu^{2+} and Cu^+ can be detected (stage a), after the first discharge to 0.01 V (stage b), Cu^{2+} was completely converted to Cu^+ and a small amount of Cu^0, then, due to the extraction of Mg^{2+}, Cu^0 and part of Cu^+ were re-oxidized to Cu^{2+} (stage c). During the subsequent second discharge process, Cu^{2+} was reduced to Cu^+ and Cu^0 (stage d). Recharge to 1.9 V, the content of Cu^{2+} began to increase (stage e). Although the incomplete conversion of Cu^{2+} causes some capacity loss during the subsequent charging and discharging process. The repeated changes of Cu valence state confirm the reversible transformation of Mg^{2+}. Combining the *ex-situ* XPS and EDS spectrum, we can infer that it is Mg^{2+} rather than $MgCl^+$ provides capacity for the full battery. In addition, we also verified the compatibility of the electrolyte with the Mo_6S_8 material, Fig. 5e shows the typical CV curves of Mg/Mo_6S_8 batteries in different electrolytes. Compared with MBP electrolyte, MFBP electrolyte demonstrated a reduced overpotential. The same conclusion can also be drawn in the subsequent charge–discharge curves (Fig. 5f). Besides, in MFBP electrolyte, the Mg/Mo_6S_8 batteries exhibited an initial discharge capacity of 120 mAh g^{-1}, and an approximately 65 mAh g^{-1} capacity over 50 cycles at 0.5C (Fig. 5g). It is worth mentioning that the rapid capacity decay in the early stage should come from a partially irreversible magnesium insertion process. However, the capacity in MBP electrolyte is only around 40 mAh g^{-1}.These experimental results further confirmed the effectiveness and practicality of the MFBP electrolyte.

3. Conclusions

In conclusion, a low-cost and effective organic boron-based electrolyte for RMBs is successfully prepared via a facile one-step reaction of

$MgCl_2$, $B(OPh)_3$ and TPFPB in THF. Based on DFT calculations on the ESP and energy orbitals, the $[TPFPB{\cdot}Cl]^-$ anion with lower HOMO energy level was proposed to increase the oxidation stability of electrolyte. Electrochemical tests indicated that the electrolyte with TPFPB additive exhibited improved magnesium ions stripping/plating efficiency (~98 %), broadening electrochemical stability windows (>3 V vs Mg/Mg^{2+}) and low polarization. Demonstrated by NMR spectroscopy, ESI-MS, XPS etc, the major equilibrium species in electrolyte were identified as tetra-coordinated boron anion $[B(OPh)_3{\cdot}Cl]^-$ and $[TPFPB{\cdot}Cl]^-$. The introduction of TPFPB also induced the formation of a stable electronically insulating MgF_2-rich SEI layer, which can effectively prevent the decomposition of electrolytes and elevate the cycle life of batteries. More importantly, the successful assembly and good performance of the Mg/CuS and Mg/Mo_6S_8 full batteries suggest the practicability of this electrolyte in RMBs. To sum up, the dual regulations for anions and SEI exhibit significant potential for designing high-efficiency RMBs electrolytes. Meanwhile, TPFPB as a multifunctional additive could find broader applications in various types of electrolytes for RMBs.

Declaration of Competing Interest

The authors declare that they have no known competing financial interests or personal relationships that could have appeared to influence the work reported in this paper.

Data availability

Data will be made available on request.

Acknowledgements

This work was supported by the National Natural Science Foundation of China (51972259, 52172231 and U1804253), the Natural Science Foundation of Hubei Province (2022CFA087), Industrialization Project of Xiangyang Technology Transfer Center of Wuhan University of Technology (WXCJ-20220017).

Appendix A. Supplementary data

Supplementary data to this article can be found online at https://doi.org/10.1016/j.cej.2023.141901.

References

[1] A. Manthiram, Materials challenges and opportunities of lithium ion batteries, J. Phys. Chem. Lett. 2 (3) (2011) 176–184.
[2] N.-S. Choi, Z. Chen, S.A. Freunberger, X. Ji, Y.-K. Sun, K. Amine, G. Yushin, L. F. Nazar, J. Cho, P.G. Bruce, Challenges facing lithium batteries and electrical double-layer capacitors, Angew. Chem. Int. Ed. 51 (40) (2012) 9994–10024.
[3] L. Zhou, K. Zhang, Z. Hu, Z. Tao, L. Mai, Y.-M. Kang, S.-L. Chou, J. Chen, Recent developments on and prospects for electrode materials with hierarchical structures for lithium-ion batteries, Adv. Energy Mater. 8 (2018) 1701415.
[4] F. Xiong, Y. Jiang, L.i. Cheng, R. Yu, S. Tan, C. Tang, C. Zuo, Q. An, Y. Zhao, J.-J. Gaumet, L. Mai, Low-strain TiP2O7 with three-dimensional ion channels as long-life and high-rate anode material for Mg-ion batteries, Interdisciplinary Mat. 1 (1) (2022) 140–147.
[5] W. Zhao, Y. Liu, X. Zhao, Z. Pan, J. Chen, S. Zheng, L. Qu, X. Yang, Chloride-free electrolytes for high-voltage magnesium metal batteries: challenges, strategies, and perspectives, Chem. Eur. J. 62 (2023) e202203334.
[6] W. Zhao, Z. Pan, Y. Zhang, Y. Liu, H. Dou, Y. Shi, Z. Zuo, B. Zhang, J. Chen, X. Zhao, X. Yang, Tailoring coordination in conventional ether-based electrolytes for reversible magnesium-metal anodes, Angew. Chem. Int. Ed. 61 (2022) e202205187.
[7] Y. Zhang, J. Li, W. Zhao, H. Dou, X. Zhao, Y. Liu, B. Zhang, X. Yang, Defect-free metal–organic framework membrane for precise ion/solvent separation toward highly stable magnesium metal anode, Adv. Mater. 34 (2022) 2108114.
[8] T. Wen, B. Qu, S. Tan, G. Huang, J. Song, Z. Wang, J. Wang, A. Tang, F. Pan, Rational design of artificial interphase buffer layer with 3D porous channel for uniform deposition in magnesium metal anodes, Energy Storage Mater. 55 (2023) 816–825.
[9] L. Zhou, Q. Liu, Z. Zhang, K. Zhang, F. Xiong, S. Tan, Q. An, Y.-M. Kang, Z. Zhou, L. Mai, Interlayer-spacing-regulated VOPO4 nanosheets with fast kinetics for high-capacity and durable rechargeable magnesium batteries, Adv. Mater. 30 (2018) 1801984.
[10] F. Xiong, S. Tan, X. Yao, Q. An, L. Mai, Crystal defect modulation in cathode materials for non-lithium ion batteries: progress and challenges, Mater. Today 45 (2021) 169–190.
[11] D. Aurbach, Z. Lu, A. Schechter, Y. Gofer, H. Gizbar, R. Turgeman, Y. Cohen, M. Moshkovich, E. Levi, Prototype systems for rechargeable magnesium batteries, Nature 407 (6805) (2000) 724–727.
[12] S. Tan, F. Xiong, J. Wang, Q. An, L. Mai, Crystal regulation towards rechargeable magnesium battery cathode materials, Mater. Horiz. 7 (8) (2020) 1971–1995.
[13] R. Deivanayagam, B.J. Ingram, R. Shahbazian-Yassar, Progress in development of electrolytes for magnesium batteries, Energy Storage Mater. 21 (2019) 136–153.
[14] H. Shuai, J. Xu, K. Huang, Progress in retrospect of electrolytes for secondary magnesium batteries, Coord. Chem. Rev. 422 (2020), 213478.
[15] S. Hou, X. Ji, K. Gaskell, P.-F. Wang, L. Wang, J. Xu, R. Sun, O. Borodin, C. Wang, Solvation sheath reorganization enables divalent metal batteries with fast interfacial charge transfer kinetics, Science 374 (6564) (2021) 172–178.
[16] H. Dong, O. Tutusaus, Y. Liang, Y. Zhang, Z. Lebens-Higgins, W. Yang, R. Mohtadi, Y. Yao, High-power Mg batteries enabled by heterogeneous enolization redox chemistry and weakly coordinating electrolytes, Nat. Energy 5 (2020) 1043–1050.
[17] J. Muldoon, C.B. Bucur, T. Gregory, Fervent hype behind magnesium batteries: an open call to synthetic chemists—electrolytes and cathodes needed, Angew. Chem. Int. Ed. 56 (2017) 12064–12084.
[18] F. Bertasi, C. Hettige, F. Sepehr, X. Bogle, G. Pagot, K. Vezzù, E. Negro, S. J. Paddison, S.G. Greenbaum, M. Vittadello, V. DiNoto, A key concept in magnesium secondary battery electrolytes, ChemSusChem 8 (18) (2015) 3069–3076.
[19] O. Mizrahi, N. Amir, E. Pollak, O. Chusid, V. Marks, H. Gottlieb, L. Larush, E. Zinigrad, D. Aurbach, Electrolyte solutions with a wide electrochemical window for rechargeable magnesium batteries, J. Electrochem. Soc. 155 (2) (2008) A103.
[20] R.E. Doe, R. Han, J. Hwang, A.J. Gmitter, I. Shterenberg, H.D. Yoo, N. Pour, D. Aurbach, Novel electrolyte solutions comprising fully inorganic salts with high anodic stability for rechargeable magnesium batteries, Chem. Commun. 50 (2) (2014) 243–245.
[21] J. Luo, S. He, T.L. Liu, Tertiary Mg/MgCl2/AlCl3 inorganic Mg2+ electrolytes with unprecedented electrochemical performance for reversible Mg deposition, ACS Energy Lett. 2 (5) (2017) 1197–1202.
[22] Y. Li, S. Guan, H. Huo, Y. Ma, Y. Gao, P. Zuo, G. Yin, A review of magnesium aluminum chloride complex electrolytes for mg batteries, Adv. Funct. Mater. 31 (2021) 2100650.
[23] H.S. Kim, T.S. Arthur, G.D. Allred, J. Zajicek, J.G. Newman, A.E. Rodnyansky, A. G. Oliver, W.C. Boggess, J. Muldoon, Structure and compatibility of a magnesium electrolyte with a sulphur cathode, Nat. Commun. 2 (2011) 427.
[24] Z. Zhao-Karger, X. Zhao, D. Wang, T. Diemant, R.J. Behm, M. Fichtner, Performance improvement of magnesium sulfur batteries with modified non-nucleophilic electrolytes, Adv. Energy Mater. 5 (2015) 1401155.
[25] D. Huang, S. Tan, M. Li, D. Wang, C. Han, Q. An, L. Mai, Highly efficient non-nucleophilic Mg(CF3SO3)2-based electrolyte for high-power Mg/S battery, ACS Appl. Mater. Interfaces 12 (15) (2020) 17474–17480.
[26] Z. Zhao-Karger, M.E. Gil Bardaji, O. Fuhr, M. Fichtner, A new class of non-corrosive, highly efficient electrolytes for rechargeable magnesium batteries, J. Mater. Chem. A 5 (22) (2017) 10815–10820.
[27] Z. Zhao-Karger, R. Liu, W. Dai, Z. Li, T. Diemant, B.P. Vinayan, C. Bonatto Minella, X. Yu, A. Manthiram, R.J. Behm, M. Ruben, M. Fichtner, Toward highly reversible magnesium–sulfur batteries with efficient and practical Mg[B(hfip)4]2 electrolyte, ACS Energy Lett. 3 (8) (2018) 2005–2013.
[28] W. Ren, D.i. Wu, Y. NuLi, D. Zhang, Y. Yang, Y. Wang, J. Yang, J. Wang, An efficient bulky Mg[B(Otfe)4]2 electrolyte and its derivatively general design strategy for rechargeable magnesium batteries, ACS Energy Lett. 6 (9) (2021) 3212–3220.
[29] O. Tutusaus, R. Mohtadi, T.S. Arthur, F. Mizuno, E.G. Nelson, Y.V. Sevryugina, An efficient halogen-free electrolyte for use in rechargeable magnesium batteries, Angew. Chem. Int. Ed. 54 (27) (2015) 7900–7904.
[30] Y.-S. Guo, F. Zhang, J. Yang, F.-F. Wang, Y. NuLi, S.-I. Hirano, Boron-based electrolyte solutions with wide electrochemical windows for rechargeable magnesium batteries, Energ. Environ. Sci. 5 (2012) 9100–9106.
[31] A. Du, Z. Zhang, H. Qu, Z. Cui, L. Qiao, L. Wang, J. Chai, T. Lu, S. Dong, T. Dong, H. Xu, X. Zhou, G. Cui, An efficient organic magnesium borate-based electrolyte with non-nucleophilic characteristics for magnesium–sulfur battery, Energ. Environ. Sci. 10 (12) (2017) 2616–2625.
[32] H. Xu, Z. Zhang, Z. Cui, A. Du, C. Lu, S. Dong, J. Ma, X. Zhou, G. Cui, Strong anion receptor-assisted boron-based Mg electrolyte with wide electrochemical window and non-nucleophilic characteristic, Electrochem. Commun. 83 (2017) 72–76.
[33] H. Xu, Z. Zhang, J. Li, L. Qiao, C. Lu, K. Tang, S. Dong, J. Ma, Y. Liu, X. Zhou, G. Cui, Multifunctional additives improve the electrolyte properties of magnesium borohydride toward magnesium–sulfur batteries, ACS Appl. Mater. Interfaces 10 (28) (2018) 23757–23765.
[34] Z. Zhang, Z. Cui, L. Qiao, J. Guan, H. Xu, X. Wang, P. Hu, H. Du, S. Li, X. Zhou, S. Dong, Z. Liu, G. Cui, L. Chen, Novel design concepts of efficient mg-ion electrolytes toward high-performance magnesium–selenium and magnesium–sulfur batteries, Adv. Energy Mater. 7 (2017) 1602055.
[35] T. Lu, F. Chen, Multiwfn: A multifunctional wavefunction analyzer, J. Comput. Chem. 33 (2012) 580–592.
[36] N. Pour, Y. Gofer, D.T. Major, D. Aurbach, Structural analysis of electrolyte solutions for rechargeable mg batteries by stereoscopic means and DFT calculations, J. Am. Chem. Soc. 133 (16) (2011) 6270–6278.

[37] S. He, J. Luo, T.L. Liu, MgCl2/AlCl3 electrolytes for reversible Mg deposition/stripping: electrochemical conditioning or not? J. Mater. Chem. A 5 (2017) 12718–12722.
[38] J. Muldoon, C.B. Bucur, A.G. Oliver, T. Sugimoto, M. Matsui, H.S. Kim, G.D. Allred, J. Zajicek, Y. Kotani, Electrolyte roadblocks to a magnesium rechargeable battery, Energ. Environ. Sci. 5 (2012) 5941–5950.
[39] S. Hermanek, Boron-11 NMR spectra of boranes, main-group heteroboranes, and substituted derivatives. Factors influencing chemical shifts of skeletal atoms, Chem. Rev. 92 (2) (1992) 325–362.
[40] Z. Chen, K. Amine, Tris(pentafluorophenyl) borane as an additive to improve the power capabilities of lithium-ion batteries, J. Electrochem. Soc. 153 (2006) A1221–A1225.
[41] G.-B. Han, J.-N. Lee, J.W. Choi, J.-K. Park, Tris(pentafluorophenyl) borane as an electrolyte additive for high performance silicon thin film electrodes in lithium ion batteries, Electrochim. Acta 56 (24) (2011) 8997–9003.
[42] S. Li, W. Zhang, Q. Wu, L. Fan, X. Wang, X. Wang, Z. Shen, Y.i. He, Y. Lu, Synergistic dual-additive electrolyte enables practical lithium-metal batteries, Angew. Chem. Int. Ed. 59 (35) (2020) 14935–14941.
[43] J. Zhao, L. Liao, F. Shi, T. Lei, G. Chen, A. Pei, J. Sun, K. Yan, G. Zhou, J. Xie, C. Liu, Y. Li, Z. Liang, Z. Bao, Y.i. Cui, Surface fluorination of reactive battery anode materials for enhanced stability, J. Am. Chem. Soc. 139 (33) (2017) 11550–11558.
[44] H.J. Lee, S.B. Kim, Y.J. Park, Enhanced electrochemical properties of fluoride-coated LiCoO2 thin films, Nanoscale Res. Lett. 7 (2012) 16.
[45] B. Li, R. Masse, C. Liu, Y. Hu, W. Li, G. Zhang, G. Cao, Kinetic surface control for improved magnesium-electrolyte interfaces for magnesium ion batteries, Energy Storage Mater. 22 (2019) 96–104.
[46] B. Xie, H.S. Lee, H. Li, X.Q. Yang, J. McBreen, L.Q. Chen, New electrolytes using Li2O or Li2O2 oxides and tris(pentafluorophenyl) borane as boron based anion receptor for lithium batteries, Electrochem. Commun. 10 (8) (2008) 1195–1197.
[47] R. Horia, D.-T. Nguyen, A.Y.S. Eng, Z.W. Seh, Using a chloride-free magnesium battery electrolyte to form a robust anode–electrolyte nanointerface, Nano Lett. 21 (19) (2021) 8220–8228.
[48] H. Dou, X. Zhao, Y. Zhang, W. Zhao, Y. Yan, Z.-F. Ma, X. Wang, X. Yang, Revisiting the degradation of solid/electrolyte interfaces of magnesium metal anodes: Decisive role of interfacial composition, Nano Energy 86 (2021), 106087.
[49] Y. Liang, H. Dong, D. Aurbach, Y. Yao, Current status and future directions of multivalent metal-ion batteries, Nat. Energy 5 (2020) 646–656.
[50] F. Xiong, Y. Fan, S. Tan, L. Zhou, Y. Xu, C. Pei, Q. An, L. Mai, Magnesium storage performance and mechanism of CuS cathode, Nano Energy 47 (2018) 210–216.
[51] Y. Shen, Y. Wang, Y. Miao, M. Yang, X. Zhao, X. Shen, High-energy interlayer-expanded copper sulfide cathode material in non-corrosive electrolyte for rechargeable magnesium batteries, Adv. Mater. 32 (2020) 1905524.
[52] W. Ren, F. Xiong, Y. Fan, Y. Xiong, Z. Jian, Hierarchical copper sulfide porous nanocages for rechargeable multivalent-ion batteries, ACS Appl. Mater. Interfaces 12 (9) (2020) 10471–10478.
[53] Z. Yao, Y. Yu, Q. Wu, M. Cui, X. Zhou, J. Liu, C. Li, Maximizing magnesiation capacity of nanowire cluster oxides by conductive macromolecule pillaring and multication intercalation, Small 17 (2021) 2102168.
[54] Y. Xie, A. Riedinger, M. Prato, A. Casu, A. Genovese, P. Guardia, S. Sottini, C. Sangregorio, K. Miszta, S. Ghosh, T. Pellegrino, L. Manna, Copper sulfide nanocrystals with tunable composition by reduction of covellite nanocrystals with Cu+ ions, J. Am. Chem. Soc. 135 (46) (2013) 17630–17637.